Metabolic Engineering 91 (2025) 204–216

Contents lists available at ScienceDirect

Metabolic Engineering

journal homepage: www.elsevier.com/locate/meteng

Harnessing CO_2 fixation and reducing power recycling for enhanced polyhydroxyalkanoates industrial bioproduction

Jing Feng [a,1], Xueshan Li [b,1], Xin Teng [a,1], Dingding Fan [a,1], Jin Yin [a], Yanci Qiu [a], Ziling Yi [a], Li Chen [b,*], Haoqian M. Zhang [a,**], Chitong Rao [a,***]

[a] Bluepha Co. Ltd., Shanghai, China
[b] Shanghai Key Laboratory of Metabolic Remodeling and Health, Institute of Metabolism & Integrative Biology, Fudan University, Shanghai, China

ARTICLE INFO

Keywords:
Cupriavidus necator
Polyhydroxyalkanoate
Reducing power
CO_2 fixation
Calvin-benson-bassham cycle

ABSTRACT

Palm oil is an attractive feedstock for bioproduction due to its high carbon content and low cost. However, its metabolism generates excess reducing power, leading to redox imbalances and reduced metabolic efficiency in industrial fermentations. Through a model-driven approach integrating flux balance analysis, we activated the Calvin-Benson-Bassham (CBB) cycle in *Cupriavidus necator* to recycle surplus reducing power and restore metabolic balance in polyhydroxyalkanoate (PHA) bioproduction. Computational simulations predicted that constitutive activation of the CBB cycle enhanced CO_2 fixation and accelerated biomass generation when utilizing palm oil as the carbon source. Model-guided optimization revealed that precise tuning of CBB activation strength was critical, as both insufficient and excessive activation led to metabolic inefficiencies. At the 2-liter bench-scale, CBB activation tuning resulted in biomass changes ranging from −18 % to 21 % and PHA yield changes ranging from −36 % to 25 %. Mechanistic studies demonstrated that CBB activation improves metabolic efficiency through reducing power recycling and carbon redistribution. In the 15 m^3 industrial-scale fermentations, the engineered strain achieved a 20 % higher PHA yield. These results demonstrate that recycling surplus reducing power is a scalable and robust strategy for enhanced bioproduction efficiency.

1. Introduction

Bio-based production leverages sustainable feedstocks to synthesize value-added molecules, offering a reduced carbon footprint compared to petroleum-based processes. Among renewable feedstocks, plant oils, such as palm oil, are particularly advantageous for commodity-scale bioproduction due to their high carbon content and relatively low cost (Sudesh et al., 2011). For the production of acetyl-coenzyme A (Acetyl-CoA)-derived molecules, plant oils and their fatty acids are superior to sugars. Unlike sugars, which lose one in three carbons through glycolysis (67 % theoretical yield), plant oils directly generate Acetyl-CoA via β-oxidation, achieving a 100 % theoretical yield (Budde et al., 2011). This metabolic efficiency makes palm oil an ideal feedstock for bioproduction processes requiring high carbon availability, such as polyhydroxyalkanoates (PHAs), which are valued for their environmental sustainability.

PHAs, a class of biodegradable and biocompatible polyesters, are among the most promising alternatives to petroleum-based plastics. These polymers have diverse applications in industries ranging from medical devices to food packaging and agriculture (Rai et al., 2021; Park et al., 2024), but their production remains economically challenging due to high raw material costs and limited productivity (Wang et al., 2014; Jiang et al., 2016; Koller and Braunegg, 2018; Yañez et al., 2020). The synthesis of PHAs relies heavily on efficient carbon utilization and reducing power supply, primarily in the forms of Acetyl-CoA and NADPH, respectively. When using highly reduced feedstocks like palm oil, excess reducing power could lead to redox imbalances and metabolic inefficiencies in PHA bioproduction.

In addition to high carbon content, plant oils are highly reduced, with a reduction degree (k = 5.75 for palm oil-derived palmitate) much

* Corresponding author. Shanghai Key Laboratory of Metabolic Remodeling and Health, Institute of Metabolism & Integrative Biology, Fudan University, Shanghai, China.
** Corresponding author. No. 210, Lane 345, Guangyue Road, Hongkou District, Shanghai, China.
*** Corresponding author. No. 210, Lane 345, Guangyue Road, Hongkou District, Shanghai, China.
E-mail addresses: chenli_imib@fudan.edu.cn (L. Chen), zhanghaoqian@bluepha.com (H.M. Zhang), raochitong@gmail.com (C. Rao).
[1] Theses authors contributed equally to this work.

https://doi.org/10.1016/j.ymben.2025.04.009
Received 27 January 2025; Received in revised form 24 March 2025; Accepted 30 April 2025
Available online 1 May 2025

higher than that of glucose or fructose (k = 4). This high reduction degree generates abundant reducing equivalents (NADH, $FADH_2$) during β-oxidation, which are vital for energy transfer and ATP generation via the electron transport chain (ETC) and oxidative phosphorylation. However, this metabolic process often results in an energy surplus, where the supply of reducing power exceeds the stoichiometric requirements for biosynthesis, resulting to inefficiencies (Dugar and Stephanopoulos, 2011). The surplus can inhibit β-oxidation, increase flux through oxidative phosphorylation, thereby increasing oxygen demand and limiting productivity in industrial fermentations constrained by oxygen transfer (Meadows et al., 2016). Addressing this challenge is critical for optimizing PHA production and ensuring the efficient utilization of highly reduced feedstocks like palm oil.

The Calvin-Benson-Bassham (CBB) cycle has emerged as a promising solution to these inefficiencies. As a natural CO_2 fixation pathway, the CBB cycle consumes reducing power and ATP, providing a mechanism to recycle surplus reducing power and restore redox balance (Schreier and Hibberd, 2019). In cyanobacteria, optimization of CBB cycle enzymes and regulatory factors has been demonstrated to enhance carbon fixation efficiency, improve energy utilization, and increase the yield of PHA production (Ciebiada et al., 2020). Similarly, studies on *Cupriavidus necator* have shown that activation of the CBB cycle enhances autotrophic growth and PHA production (Li et al., 2020; Kim et al., 2022). Furthermore, CO_2 reutilization from sugar degradation has been associated with increased PHA yields (Shimizu et al., 2015).

Despite these advancements, the exploration of CBB cycle activation within heterotrophic systems for PHA production remains underexplored, particularly under industrially relevant conditions where energy-dense palm oil is used and oxygen supply is constrained. Additionally, scaling CBB activation strategies from laboratory settings to large-scale fermentation systems has not been practically demonstrated. Addressing these gaps is essential for realizing the full potential of CBB-mediated reducing power recycling in industrial bioproduction.

In this study, we activated the CBB cycle in *C. necator* H16G to recycle excess reducing power generated during palm oil metabolism. Our research systematically analyzes the effects of CBB activation strength, revealing that precise tuning is critical for balancing reducing power recycling with biosynthetic demands, thereby maximizing PHA production. We validated this approach in both pilot-scale (200-L) and industrial-scale (15-m^3) bioreactors, exploring the scalability and robustness of the strategy. This study also highlights the broader applicability of integrating CO_2 fixation to address redox imbalances caused by highly reduced feedstocks, paving the way for sustainable production of other high-value compounds in microbial systems.

2. Methods

2.1. Strain and culture media

The bacteria used in this study were *C. necator* H16G (an H16 mutant able to grow in glucose and produce PHB) (Orita et al., 2012) and mutants derived from this strain. The rich medium used for growth of *C. necator* H16G was TYGA media (10 g/L tryptone, 5 g/L yeast extract, 3 g/L glucose and 3 g/L ammonium sulfate) and TYOA media (10 g/L tryptone, 5 g/L yeast extract, 1.5 g/L palm oil and 3 g/L ammonium sulfate). The concentrations of salts in the *C. necator* H16G minimal medium have been reported previously (Tang et al., 2020). Carbon and nitrogen sources were added to the minimal medium as described in the text. The carbon sources used in this study were glucose and palm oil. Chemicals were purchased from Sinopharm Chemical Reagent Co., Ltd. (Shanghai, China) unless noted otherwise. *C. necator* H16G strains were always grown aerobically at 30 °C.

2.2. Fermentation conditions and waste gas component analysis

C. necator H16G strains were cultured from single colony in TYGA media for 12 h as a primary seed culture. These cultures were inoculated at 1 % into TYOA media for 14 h as second seed culture. Subsequently, this precultures were used to inoculate at 10 % (v/v) into the bioreactor with minimum media supplemented with 2.5 g/L yeast extract, 4 g/L ammonium chloride and palm oil as nitrogen and carbon sources. The temperature of bioreactors was kept constant at 30 °C. The pH of each culture was maintained at 6.8 through controlled addition of 28 % ammonium solution. Stirring was controlled at speeds of 300 to 1500 rpm. The dissolved oxygen concentration was maintained above 20 % by adjusting aeration. The feeding rate of oil feedstock during fermentation was adjusted by measuring the residual fatty acids through hexane extraction of the fermentation broth. The waste gas of 200-L and 15-m^3 bioreactor was directed to Prima BT bench top process mass spectrometer (Thermo Fisher, USA) for gas component analysis.

2.3. Plasmid and strain construction

In this study, General genetic manipulations were performed according to the standard procedures. DNA was routinely amplified by using PrimerSTAR Max DNA polymerase (Takara, China) and digested using restriction enzymes from New England BioLabs, USA. Gibson assembly (Gibson et al., 2009) was used for plasmid constructions. Plasmids were transformed into *C. necator* H16G strains via transconjugation with *Escherichia coli* S17-1. Markerless gene deletions and insertions in the *C. necator* genome were achieved following the protocol described by Insomphun et al. (2014). The strains and plasmids used in this study are described in Table 1. The sequences of all oligonucleotide primers used in this study are provided in Table S1 in the supplemental material.

2.4. PHA assays via gas chromatography (GC)

The bacterial cells were harvested and centrifuged at 10,000 g for 10 min. Dry cell weight (DCW) were determined after drying. The PHA contents were then analyzed using gas chromatography (GC-2010 Pro, SHIMADZU, Japan) as previously described (Sheu and Lee, 2004).

Table 1
Strains and plasmids used in this study.

Strains or plasmids	Description	Source or reference
Cupriavidus necator		
H16G	Parental strain	Orita et al. (2012)
*cbbR**	Δ*proC*Δ*cbbR*, with stable plasmid with the double mutant *cbbR* gene (G205D, G118D) introduced	This study
cbb1 ~ cbb7	Replacing the chromosomal *cbbR-PcbbLS* regulatory sequence with constitutive promoters of various strength	This study
Escherichia coli		
DH5α	General cloning strain	Invitrogen, USA
S17-1	Strain for conjugative transfer of plasmids to *C. necator*	Simon et al., 1983
Plasmids		
pK18mob	The backbone used to make other plasmids for gene deletion/insertion in *C. necator* genome	Orita et al. (2012)
pKO-ΔproC	Plasmid for deletion of *proC* from *C. necator* genome	This study
pKO-ΔAcbbR	Plasmid for deletion of *cbbR* from *C. necator* genome	This study
pSP-proC-cbbR (G205D/G118D)	Plasmid for introducing *cbbR* mutant into *C. necator*	This study
pKO-L-p1 ~ pKO-L-p7	Plasmid for introducing constitutive promoters with various strength into *C. necator* genome	This study

2.5. Metabolomics analysis

C. necator H16G and cbb4 samples in 2-L fed-batch cultures were collected at 10 h and 32 h using 2.0 mL grinding tubes (Jingxin, China). Each grinding tube was added with 405 μL of the reagent prepared by mixing MEOH and H_2O at a ratio of 5:4, two 3.2 mm grinding beads (Jingxin, China), and 750 μL methyl tert-butyl ether (MTBE). The homogenate was ground using a grinder (Jingxin, China) at 4 °C, 30 Hz, for 15 s × 4 times with an interval of 15 s. The sample was then centrifuged in a centrifuge (Eppendorf 5435R, Germany) at 21,130 g for 10 min at 4 °C. 100 μL of the lower phase metabolite fraction was taken out, diluted with 300 μL of ACN:MEOH (1:1), and placed in a −80 °C refrigerator overnight for protein precipitation. Before injection, the sample was centrifuged at 21,130 g for 10 min, and then 100 μL was transferred into an injection vial for metabolomics LC-MS analysis. An equal-proportion sampling from each test sample was mixed to form a quality control (QC) for evaluating the instrument stability.

Untargeted metabolomics data acquisition was performed using a Shimadzu LC system coupled to a TripleTOF mass spectrometer (QTOF 6600+, ABSciex, made in Woodlands Central Industrial Estate, Singapore). Chromatographic separation was achieved using a HILIC column (IHILIC-(P) Classic column, 5 μm, 150 mm × 2.1 mm, 200 A, made in Sweden). The mobile phase A was 20 mmol/L ammonium acetate, 0.1 % ammonium hydroxide, and 2.5 μmol/L methylene diphosphate in 95:5 water:ACN, and mobile phase B was acetonitrile. The gradient was as follows: 0 min, 85 % B; 2 min, 85 % B; 7 min, 65 % B; 12 min, 35 % B; 12.1 min, 20 % B; 15.9 min, 20 % B; 16 min, 85 % B; 23 min, 85 % B. The flow rate was set at 0.2 mL/min with a sample injection volume of 5 μL and the total run time at 23 min. ESI parameters setup was GS1, 60; GS2, 60; CUR, 35; temperature, 500; ISVF, −4500 in negative modes. Peak area for each metabolite was integrated using El-MAVEN software (version 0.12.1).

2.6. ^{13}C isotope tracing of central carbon metabolites

C. necator H16G and *cbbR** were grown and maintained in TYGA medium, in an orbital shaker incubator at 200 rpm. Cells in mid-exponential phase were used to inoculate at an initial OD(600) of 0.1 into minimal media supplemented with the 1.0 % (v/v) palm oil, 0.9 g/L polyglycerol ester of oleic acid, 1 g/L NH_4Cl and 0.5 g/L yeast extract. During the cultivation process, $NaH^{13}CO_3$ was added every 2 h during the fermentation from 12 h to 24 h with a final concentration of 5 mM. 1-mL of sample were collected by centrifuge at 4 °C and washed with PBS twice. Cell pellets were resuspended in 80 % methanol, lysed by sonication (JY92-IIN,NingBo Scientz Biotechnology Co., Ltd.) and centrifuged at 4 °C, 18000 g for 15 min. The supernatant was concentrated (Labconco, Kansas City, MO, USA) and 100 μL of 80 % methanol was added to reconstitute metabolites for analysis.

^{13}C labeling data acquisition was performed at Metabo-Profile (Shanghai, China) using triple quad mass spectrometry (ACQUITY-I UPLC/Xevo TQS, Waters, USA). Chromatographic separation was achieved using 4.6-mm column, Amide XBridge (Waters, USA) at 40 °C. The mobile phase A was 5 % acetonitrile, 20 mM ammonium hydroxide and 20 mM ammonium acetate, and mobile phase B was acetonitrile. The gradient was as follow: 0∼3.5 min, 85∼32 % B; 3.5–12 min, 32∼2 % B; 12–16.5 min, 2 % B; 16.5–17 min, 2–85 % B; 17∼25.5 min, 85 % B. The flowrate was set at 0.4 mL/min with a sample injection volume of 5 μL. The ESI was set at negative mode, 2.5 kv, source temperature at 150 °C, desolvation tempareture at 500 °C and desolvation gas flow at 1000 L/h. Data were analyzed with MassLynx v4.1 (Waters, USA). All MS grade reagent were from Merck Chemicals, Germany.

All data from labeling experiments were subjected to natural abundance correction.

2.7. Estimation of Acetyl-CoA labeling pattern

The labeling patterns of malate and citrate were used to infer the acetyl-CoA labeling distribution, specifically focusing on the acetyl group of acetyl-CoA (Zhang et al., 2021). Let the labeling patterns of malate, acetyl-CoA acetyl group, and citrate be represented as follows:

Malate labeling pattern: [M_0, M_1, M_2, M_3, M_4]

Acetyl-CoA acetyl group labeling pattern: [A_0, A_1, A_2]

Citrate labeling pattern: [C_0, C_1, C_2, C_3, C_4, C_5, C_6]

The labeling patterns of citrate are expressed as a linear combination of the labeling patterns of malate and the acetyl group of acetyl-CoA:

$$C_0 = M_0A_0$$

$$C_1 = M_0A_1+M_1A_0$$

$$C_2 = M_0A_2+M_1A_1+M_2A_0$$

$$C_3 = M_1A_2+M_2A_1+M_3A_0$$

$$C_4 = M_2A_2+M_3A_1+M_4A_0$$

$$C_5 = M_3A_2+M_4A_1$$

$$C_6 = M_4A_2$$

Then least squares regression was used to solve the equations to obtain the best estimates for the labeling distribution of the acetyl group in acetyl-CoA.

2.8. PHA extraction and ^{13}C enrichment analysis

Cellular PHA was labeled the same as central metabolites except the cells were harvested at 36 h. Soxhlet extraction method (Palmieri et al., 2021) was used to extract PHA from *C. necator* strains. In brief, cell pellet was repeatedly brought into contact with chloroform in a distillation flask for 2 h. The organic phase was then completely separated from the biomass and removed under air blow. The extracted PHA was then analyzed by elemental analyzer - isotope ratio mass spectrometry (EA-IRMS) at Shenzhen Customs Food Inspection and Quarantine Technology Center (Shenzhen, China) following the institute internal analytical protocols.

2.9. Stoichiometric calculations of the impact of CBB-mediated CO_2 fixation on PHA yields

The stoichiometric calculation for polyhydroxybutyrate (PHB) monomer, 3-hydroxybutyrate (3HB) yield and oxygen consumption without CBB activation used the following formula:

$$\mathbf{1}\ CH_3(CH_2)_{14}COOH + \mathbf{5}\ O_2 \rightarrow \mathbf{4}\ 3HB + \mathbf{4}\ H_2O + \mathbf{3}\ NAD(P)H + \mathbf{7}\ FADH_2$$

The optimal CBB activation strength was defined as the condition where all available NADH was utilized for carbon fixation (and available $FADH_2$ utilized for ATP generation). The stoichiometric calculation of the total carbon fixed under this optimal activation strength used the following formula:

$$\mathbf{3}\ NAD(P)H + \mathbf{1.33}\ CO_2 + \mathbf{2.67}\ ATP \rightarrow \mathbf{0.33}\ 3HB + \mathbf{0.67}\ ADP + \mathbf{2}\ AMP$$

The stoichiometric calculation for 3HB yield and oxygen consumption with optimum CBB activation used the following formula:

$$\mathbf{1}\ CH_3(CH_2)_{14}COOH + \mathbf{3.5}\ O_2 + \mathbf{1.33}\ CO_2 \rightarrow \mathbf{4.33}\ 3HB + \mathbf{3}\ H_2O$$

2.10. Transcriptomics analysis

The samples of *C. necator* H16G and its mutants were collected at 10 h and 32 h of 2-L fed-batch fermentation and total RNA was isolated

from the cell pellet with Trizol reagent (Invitrogen, USA) according to manufacturer's instructions. Total RNA was used as input material for the RNA sample preparations. Sequencing libraries were generated using NEBNext Ultra RNA Library Prep Kit for Illumina (NEB, USA, Catalog #: E7530L) following manufacturer's recommendations and index codes were added to attribute sequences to each sample. The qualified libraries were pooled and sequenced on Illumina platforms with PE150 strategy in Novogene Bioinformatics Technology Co., Ltd (Beijing, Chisana), according to effective library concentration and data amount required.

Gene expression is calculated with nf-core/rnaseq ioinformatics pipeline (Ewels et al., 2020) in the process. After read quality control, adapter trimming, removal of ribosomal RNA, reads were aligned to reference genome of *C. necator* H16G(GCA_000009285.2) with the aliger STAR (Dobin et al., 2013). Further, reported gene expression values were quantified as TPM (transcripts per million) with Salmon (v1.10.1) (Patro et al., 2017).

2.11. Proteome analysis

Cell pellet of *C. necator* H16G fermented in 200-L bioreactor obtained by centrifugation. Proteins were extracted from wet cell pellets by adding five volumes of lysis buffer (40 mM Tris-HCl, 8 M urea, 10 mM DTT, and protease inhibitors) and homogenized on ice with intermittent sonication. The lysates were centrifuged at 15,000 g for 30 min at 4 °C, and the supernatant was collected. For digestion, protein samples were incubated at 37 °C for 4 h for denaturation, followed by alkylation with DTT and IAM (1:5:n ratio) in the dark for 1 h. The samples were diluted with 50 mM ammonium bicarbonate (pH 8.0) to reduce the urea concentration to below 1 M, and trypsin was added at a 50:1 (protein: enzyme) mass ratio for digestion at 37 °C for 20 h. The reaction was quenched with 0.5 % formic acid. Peptides were desalted using Sep-Pak C18 solid-phase extraction columns (Waters, USA), activated with 2 mL of 1 % formic acid, and equilibrated with 2 mL of 0.1 % formic acid. The digested samples were loaded onto the SPE columns, washed with 2 mL of 0.1 % formic acid to remove salts, and eluted with 2 mL of 80 % acetonitrile containing 0.1 % formic acid. The eluted peptides were dried and resuspended with 0.1 % formic acid solution.

Before injection, the sample was centrifuged at 15,000 rpm for 30 min, and transferred into an injection vial for LC-MS analysis. Proteomics data acquisition was performed using a Easy nLC1000 LC system (Thermo Fisher, USA) coupled to a orbitrap mass spectrometer (Thermo Fisher, USA). Chromatographic separation was achieved using Acquity UPLC BEH C18 column, (1.7 μm, 100 mm × 2.1 mm, 130 A, USA). The mobile phase A was 0.1 % formic acid, and mobile phase B was 0.1 % formic acid in acetonitrile. The gradient was as follows: 0 min, 5 % B; 65 min, 30 % B; 70 min, 100 % B; 75 min, 100 % B. The flow rate was set at 0.3 mL/min with a sample injection volume of 1 μL. The ionization was set to positive mode with a default precursor charge of 2. The full MS scan was conducted at a resolution of 60,000 with an AGC target of 3e6 and a maximum injection time (IT) of 100 ms. The scan range covered 350–2000 m/z. For the data-dependent MS/MS (dd-MS2), a resolution of 15,000 was used with an AGC target of 1e5 and a maximum IT of 50 ms. The loop count was set to 20, and the isolation window was 2.0 m/z. The stepped normalized collision energy (NCE) was set to 28. Dynamic exclusion was applied for 50 s with a minimum AGC target of 8.00e3 and an intensity threshold of 1.6e5. Apex-triggering and preferred peptide matching were enabled for optimal fragmentation. Data were analyzed with Xcalibur software.

The proteome analysis of *C. necator H16G* (GCF_000009285.2) was the performed using Proteome Discoverer 2.2 (PD2.2) and Spectronaut software (Martinez-Val et al., 2021). DDA scan mode data obtained from the mass spectrometer were subjected to database searching using PD2.2. The search parameters included a mass tolerance of 10 ppm for precursor ions and 0.02 Da for fragment ions. Fixed modifications were set as alkylated cysteine, and variable modifications included methionine oxidation and N-terminal acetylation. Up to 2 missed cleavage sites were allowed during the search. To improve the quality of the analysis results, PD2.2 software further filtered the search results. Peptide Spectrum Matches (PSMs) with a confidence level above 99 % were considered reliable PSMs. Proteins that contained at least one unique peptide segment were considered reliable proteins. Only the reliable PSMs and proteins were retained, and false discovery rate (FDR) validation was performed to remove peptide segments and proteins with an FDR greater than 1 %. The identified proteins from PD2.2 were imported into Spectronaut software (version 14.0, Biognosys) to generate a spectral library. Peptide and ion pair selection rules were applied to choose the corresponding peptide segments and sub-ions from the spectra, generating a Target List. DIA data was then imported, and ion pairs were extracted based on the Target List. Sub-ion matching and peak area calculations were performed, enabling simultaneous qualitative and quantitative analysis of the peptide segments. iRT was used for retention time calibration, and a precursor ion Q-value cutoff of 0.01 was set.

2.12. Flux balance analysis (FBA)

The genome-scale metabolic model of *C. necator* H16G used was iCN1361, derived from Pearcy et al. (2022). In order to predict NADH amount, we incorporated a reaction to the spontaneous hydrolysis of NADH: R_NADHez: M_NADH → M_NAD + M_PROTON. FBA was performed utilizing COBRApy (Ebrahim et al., 2013) for FBA and FVA simulations with the GLPK and CPLEX 12.8 as the linear optimization solver. Custom code used in this study is available at https://github.com/DingDingFan/CBB_paper/tree/main/FBA.

2.13. Resource balance analysis (RBA)

The RBA model for *C. necator* H16G was derived from Jahn et al. (2021) with adjusted biomass yield at an expense of 30.299 ATP mmol $g{\cdot}DCW^{-1}{\cdot}h^{-1}$, with no ATP consumption for protein synthesis. The maintenance ATP for the cell was also modified to a constant 3 ATP mmol $g{\cdot}DCW^{-1}{\cdot}h^{-1}$ in accordance with the latest 2022 GSM (Genome-scale Metabolic Models) version. In addition, the model was also calibrated for using palmitate as substrate by adding estimates for k_{app}, the apparent catalytic rate for each metabolic enzyme, following the procedure outlined in https://m-jahn.github.io/R-notebook-ralstonia-proteome/Ralstonia_model_constraints.nb.html. For each model reaction and substrate limitation, flux boundaries were obtained from Flux Sampling Analysis (FSA) using COBRApy (Ebrahim et al., 2013), with a substrate uptake rate of 0.745 mmol $g{\cdot}DCW^{-1}{\cdot}h^{-1}$. Concurrently, the proteome obtained was used to estimate enzyme levels. The relative protein mass fraction was determined by dividing MS intensity per protein by sum of all intensities. The mass fraction (g/g total protein) was then converted to protein concentration in mmol/gDCW by multiplying it with estimated protein concentration of 0.65 g protein/gDCW (Jahn et al., 2021), and then dividing by molar mass of each protein (g/mol). To compute the reducing power, we also added a reaction to the spontaneous hydrolysis of NADH as described in FBA. RBA model was generated using the RBApy (Bulović et al., 2019).

2.14. Carbon flow calculation

Carbon flow analysis was performed to quantify the distribution of carbon derived from palm oil during the fermentation process. Palm oil was used as the sole carbon source, with its composition defined as $C_{17.24}H_{33.1}O_2$ and a molecular weight of 271.98 g/mol. The major output components included PHA, residual cell weight (RCW), and CO_2. The compositions and molecular weights of these outputs were as follows: PHA ($C_4H_6O_2$, Mw = 86 g/mol), RCW ($CH_{1.74}O_{0.46}N_{0.19}$, Mw = 23.76 g/mol), and CO_2 (Mw = 44 g/mol). The carbon content of each component was calculated based on their molecular composition.

The total carbon input from palm oil was calculated as:

$$\text{Toal carbon input (g)} = \text{Pallm oil consumed (kg)} \times 0.76$$

where 0.76 is the carbon content per unit mass of palm oil.

The output carbon distribution was calculated as follows.

1. CO_2 Carbon Output:

$$CO_2 \text{ carbon output (g)} = CO_2 \text{ produced (kg)} \times 0.27$$

$$CO_2 \text{ carbon fraction} = \frac{CO_2 \text{ carbon output (g)}}{\text{Total carbon input (g)}}$$

2. PHA Carbon Output:

$$\text{PHA carbon output (g)} = \text{DCW (g/L)} \times \text{Fermentation volume (L)} \times \text{PHA content fraction} \times 0.56$$

$$\text{PHA carbon fraction} = \frac{\text{PHA carbon output (g)}}{\text{Total carbon input (g)}}$$

3. Cellular Carbon Output:

$$\text{Cellular carbon output (g)} = \text{DCW (g/L)} \times \text{Fermentation volume (L)} \times (1 - \text{PHA content fraction}) \times 0.51$$

$$\text{Cellular carbon fraction} = \frac{\text{Cellular carbon output (g)}}{\text{Total carbon input (g)}}$$

4. Others:

$$\text{Others} = 1 - CO_2 \text{ carbon fraction} - \text{PHA carbon fraction} - \text{Cellular carbon fraction}$$

The sum of carbon fractions for CO_2, PHA, and RCW was validated to ensure consistency with the input carbon. This approach allowed for the detailed quantification of carbon flow from palm oil into cellular biomass, bioproduct synthesis, and respiratory CO_2 emission under the tested fermentation conditions.

3. Results

3.1. Revealing excess reducing power through theoretical modeling of palmitate metabolism in C. necator H16G

Different carbon sources produce varying amounts of acetyl-CoA and reducing equivalents, both of which are essential for biomass growth and industrial biomolecule synthesis, including PHA. Stoichiometric analysis showed that palmitate metabolism via the fatty acid β-oxidation (FAO) pathway generates significant higher levels of acetyl-CoA and reducing equivalents ($C_{16}H_{32}O_2 \rightarrow 8$ Acetyl-CoA + 7 NADH + 7 $FADH_2$) compared to fructose metabolism via the Entner–Doudoroff (ED)

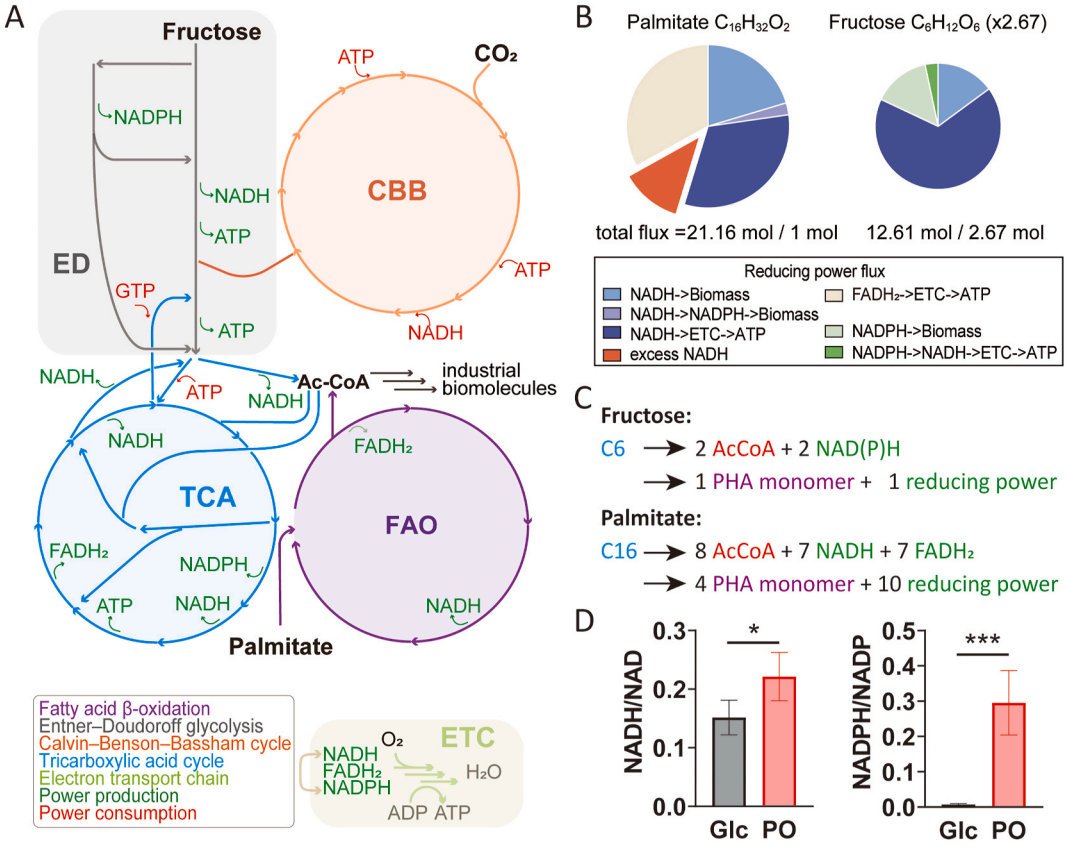

Fig. 1. Reducing power flux during metabolism of palmitate and fructose. **(A)** Schematic representation of the central metabolic pathways in *C. necator* utilizing palmitate or fructose as carbon sources. Energy production (green) and consumption (red) are highlighted. **(B)** Excess reducing power in the form of NADH during bioconversion of palmitate, but not fructose, into cellular biomass, revealed by metabolic modeling using flux balance analysis. Note that for comparison, flux of carbon source is set at 1 mol for palmitate and 2.67 mol for fructose. **(C)** Stoichiometric calculations for PHA production show that palmitate metabolism generates considerably more NADH equivalent surplus than fructose metabolism. (D) NADH/NAD and NADPH/NADP ratios in *C. necator* H16G cultured with glucose (Glc) or palm oil (PO) as the carbon source for 10 h in a 2-L fed-batch fermentation. (For interpretation of the references to colour in this figure legend, the reader is referred to the Web version of this article.)

glycolysis pathway (2.67 $C_6H_{12}O_6$ → 5.33 Acetyl-CoA + 5.33 CO_2 + 8 NADH + 2.67 NADPH). Using flux balance analysis (FBA) with a genome-scale metabolic model of *C. necator* H16G, we simulated optimal flux distributions in the context of biomass accumulation, and quantified the production and consumption of reducing equivalents and ATP (Jahn et al., 2021) (Fig. 1A). To facilitate comparisons of energy between different forms and varied growth conditions, here we take advantage of the biologically feasible interconversions between energy forms (NADPH ↔ NADH via transhydrogenases, and NADPH/NADH/-$FADH_2$ → ATP via electron transport chain) and make an artificial assumption that NADH is the last form of energy consumed for biomass generation (see methods). FBA analysis revealed that palmitate metabolism at the biomass growth stage yields 2.58 mol of NADH per 1 mol of substrate in excess, accounting for 18.2 % of the total NADH flux (Fig. 1B). Introducing a pseudo-reaction to dispose of the excess NADH did not affect biomass generation rates, consistent with the presence of an energy surplus. In contrast, fructose metabolism did not result in excess NADH relative to anabolic requirements of biomass growth, and enforcing the NADH disposal reaction negatively affected biomass generation. These findings for fructose metabolism are consistent with prior proteome studies using resource balance analysis (RBA), another advanced model incorporating enzyme abundance and kinetic parameters (Jahn et al., 2021). To validate the observations from FBA, RBA was further applied to quantify energy fluxes, confirming that palmitate metabolism resulted in an excess of reducing power, while fructose metabolism did not (Fig. S1).

In the context of PHA synthesis, specifically poly-3-hydroxybutyrate (PHB) produced by *C. necator* H16G in this study, stoichiometric calculations showed that palmitate metabolism generates substantially more reducing power than fructose (Fig. 1C). Experimental measurements further confirmed this prediction, showing that both NADH/NAD and NADPH/NADP ratios were markedly higher when *C. necator* H16G was cultured with palm oil compared to glucose, providing direct evidence of excess reducing power accumulation (Fig. 1D).

Together, these results suggested that while the high carbon content and reducing power in palm oil offer potential advantages for PHA bioproduction, the excess reducing power generated from palmitate metabolism may affect cell growth and bioproduction of target compounds such as PHA.

3.2. CO_2 fixation enhances biomass production through CBB cycle activation in *C. necator* H16G

We wonder if we can leverage the excess reducing equivalents for additional biomass and biomolecule production. One feasible approach is CO_2 biofixation, which demands significant reducing power and ATP. We took advantage of the endogenous Calvin-Benson-Bassham (CBB) cycle in *C. necator* H16G, a metabolic pathway capable of fixing CO_2 to support lithoautotrophic growth and PHA production. RNAseq was performed to assess the transcriptional activity of the *cbb* genes during growth in palm oil. In contrast to moderate expression levels observed during growth on fructose (Shimizu et al., 2013), transcription of the *cbb* genes was strongly repressed in palm oil during both the early growth phase and the late PHA production phase (Fig. 2A, Fig. S2). This finding suggests that transcriptional activation is crucial for the reutilization of reducing power. Previous studies on *C. necator* revealed that the regulation of the CBB promoter P*cbbLS* involves sigma 70 factors (Kusian et al., 1995), intermediary metabolites such as phosphoenolpyruvate (Grzeszik et al., 2000), the two-component regulatory system RegA/B (Gruber et al., 2017), and, critically, *cbbR*, a LysR-type transcriptional regulator located upstream of the CBB cluster (Windhövel and Bowien, 1991; Bowien and Kusian, 2002). We engineered the transcriptional regulator *cbbR* by knocking out the chromosomal *cbbR* and introducing an ectopic, constitutively active *cbbR** variant with point mutations G205D and G118D (Dangel and Tabita, 2015). RNAseq profiling of the *cbbR** mutant revealed an average of 50-fold transcriptional upregulation of the *cbb* genes compared to the wildtype H16G, with minimal perturbation to other genes involved in central carbon metabolism (Fig. 2A, Fig. S2).

To evaluate the impact of *cbbR**-mediated CBB activation, *C. necator* H16G and its *cbbR** mutant were compared in the 2-L bench-scale fermentation using palm oil as the fed-batch feedstock. Quantitative analysis of oil consumption, dry cell weight (DCW), and PHA production demonstrated that the *cbbR** mutant exhibited significantly enhanced substrate utilization, biomass accumulation and PHA synthesis compared to the wildtype strain (Fig. 2B). However, this enhancement was not observed when fructose was used as the substrate (Fig. S3), indicating that the metabolic advantage conferred by CBB activation is specific to palm oil metabolism. These findings suggest that CBB pathway activation enhances PHA biosynthesis efficiency under palm oil-fed conditions, likely by mitigating excess reducing power accumulation.

To verify if CBB activation leads to CO_2 fixation, both strains were grown in a medium with palm oil as the main carbon source and supplemented with ^{13}C-labeled sodium bicarbonate. Analysis of ^{13}C-labeled central carbon metabolites showed that the *cbbR** mutant exhibited significantly higher ^{13}C labeling percentages compared to the wildtype H16G (Fig. 2C–S4A), especially in in 3-phosphoglycerate (3 PG) and its downstream metabolites, confirming effective carbon fixation by Rubisco, the key enzyme of the CBB cycle. The average ^{13}C labeling percentages in the CBB and Entner-Doudoroff (ED) pathways increased by 2.65-fold in the *cbbR** mutant compared to H16G, while the TCA cycle exhibited a 1.97-fold increase. The relatively lower increase in TCA cycle labeling was likely due to the metabolic input from β-oxidation of unlabeled palm oil, and loss of ^{13}C labeled carbon during TCA cycle turning. Together, these data support the successful activation of the CBB pathway by *cbbR** modification, redirecting fixed CO_2 into central metabolism.

We examined the contribution of CO_2 fixation to acetyl-CoA, the precursor for PHA biosynthesis. The ^{13}C-labeled fractions of the acetyl group of acetyl-CoA were estimated from malate and citrate due to the difficulty of direct measurement (the CoA moiety was labeled and oxaloacetate was undetectable). The acetyl group of acetyl-CoA showed 4.8 % and 10.6 % ^{13}C labeling percentages in H16G and *cbbR**, respectively (Fig. 2D–S4B), indicating that a portion of the fixed carbon is channeled into acetyl-CoA biosynthesis. Significant elevation of ^{13}C-labeled fraction was also observed in purified PHA after 36 h fermentation (Fig. 2E). These findings suggested that the activated CBB pathway successfully fixes CO_2 and contributes to PHA biosynthesis.

3.3. Fine-tuning CBB activation strength maximizes biomass and PHA production

While the plasmid-based expression of *cbbR** successfully activated the CBB pathway and improved PHA production, its limitation became evident as the PHA yield showed a progressive decline across successive fermentation batches (Fig. S5). This decline, attributed to the instability of plasmid maintenance and expression during prolonged industrial operations, prompted us to use a genome integrated biorthogonal design for CBB activation to achieve more reliable and sustainable bioproduction.

To investigate the impact of CBB activation strength on cell growth and PHA production, we first performed stoichiometric calculations to evaluate how enforcement of CBB-mediated CO_2 fixation could impact PHA yields. Recycling the excess NADH derived from palmitate metabolism fully into CBB-mediated CO_2 fixation was predicted to improve PHA yields by 8.25 % (Table 2). Consistent with this stoichiometry, metabolic modeling using FBA and RBA predicted a 2.19–4.98 % increase in biomass generation rates from palmitate at optimal CBB strength, defined as the optimal flux of CBB-mediated CO_2 fixation (Fig. 3A, Fig. S6). Biomass generation rates were lower at suboptimal CBB strengths, either because excess reducing power remained unused

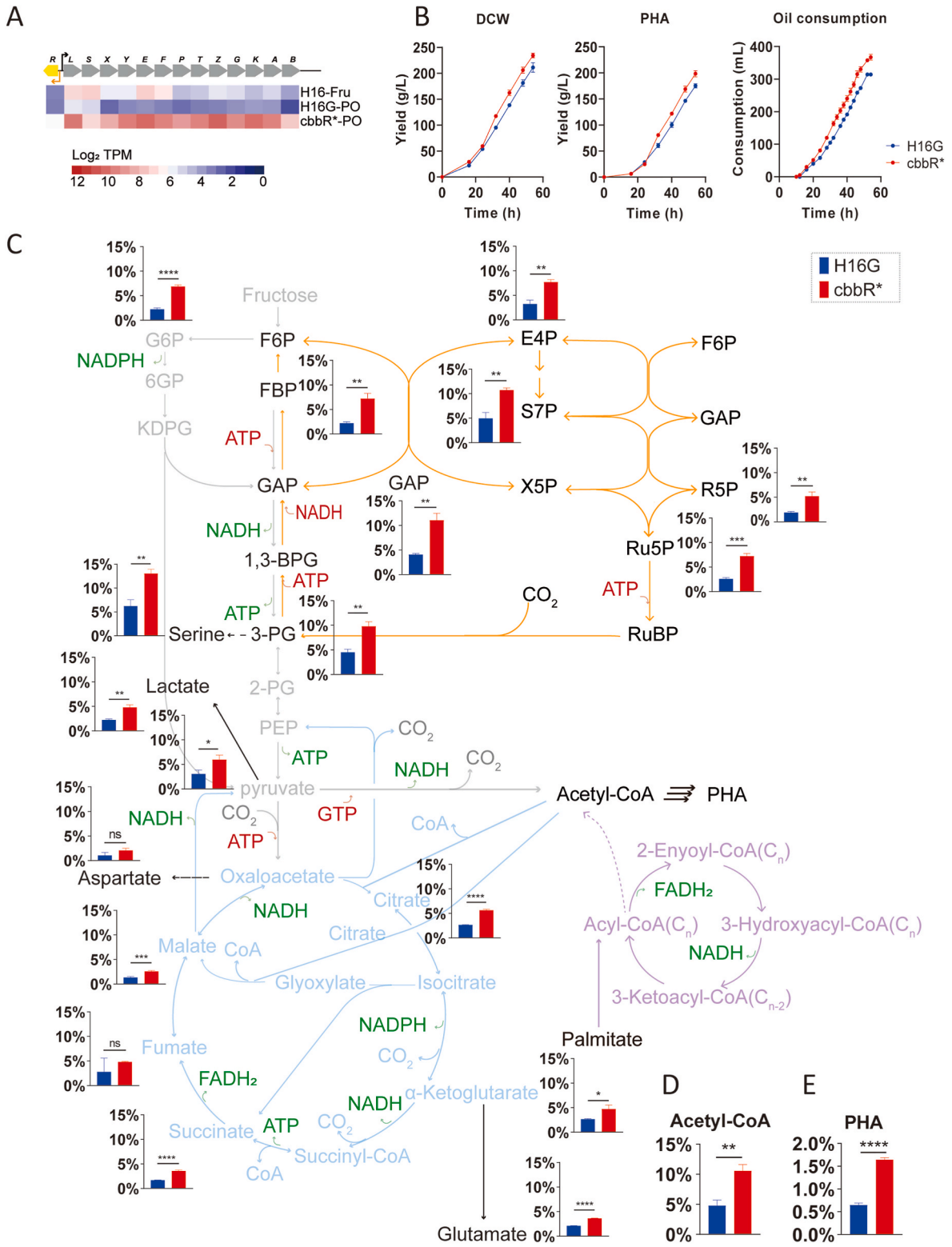

Fig. 2. CBB pathway activation enhances CO_2 fixation and biomass generation under reducing power surplus. **(A)** Transcriptional levels (transcripts per million, TPM) of the chromosomal CBB cluster in *C. necator* H16/H16G and *cbbR** strains during growth on fructose or palm oil. For fructose, RNAseq data at 16 h were acquired from a previous study (Shimizu et al., 2013); for palm oil, samples were collected at 10 h. The *cbbR** activation resulted in significantly higher transcriptional levels compared to the wildtype strain. **(B)** Biomass (dry cell weight, DCW), PHA yield, and oil consumption curves for *C. necator* H16G and *cbbR** strains in 2-L bench-scale fermentation using palm oil as the carbon source. **(C)** ^{13}C labeling percentage in central carbon metabolites at 24 h post inoculation. **(D)** Estimated ^{13}C labeling percentage in acetyl-CoA, calculated from malate and citrate due to the inability to directly measure oxaloacetate. **(E)** ^{13}C labeling percentage in PHA at 36 h post inoculation. All labeling experiment were done by supplementing 5 mM ^{13}C-labeled sodium bicarbonate every 2 h from 12 to 24 h during palm oil fermentation. Data are shown as mean ± SEM, n = 3 per group. Statistical significance was determined using a two-tailed Student's t-test (ns not significant, *p < 0.05, **p < 0.01, ***p < 0.001, ****p < 0.0001).

Table 2
Effect of reducing power recycling on theoretical PHA yield and O_2 requirement.

CBB activation Strength	Minimum mol Palmitate consumption per mol 3HB	Maximum mol 3HB yield per mol Palmitate	Minimum mol O_2 consumption per mol 3HB	Maximum productivity g/(L*h) under 100 mmol/(L*h) O_2 supply limit
0 %	0.25	4	1.25	6.88
Optimum	0.23	4.33 (+8.25 %)	0.81	10.65 (+55 %)

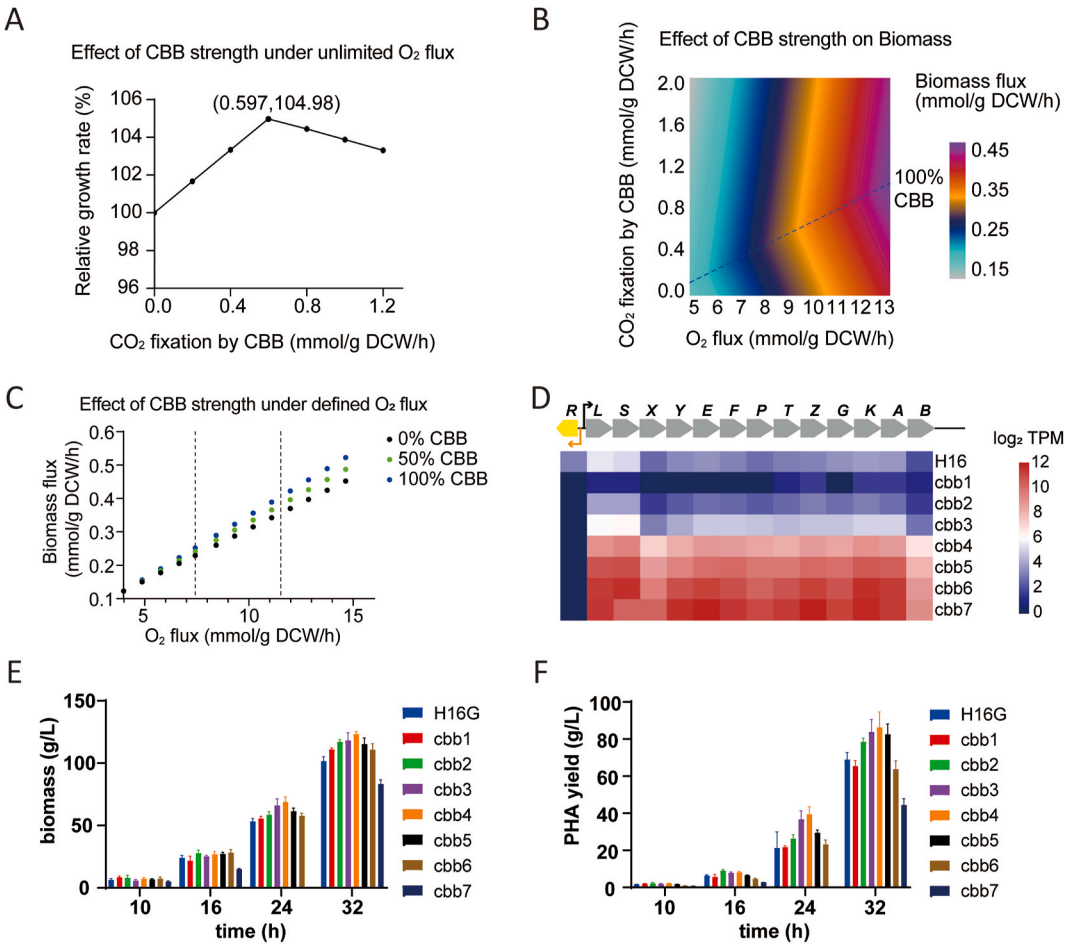

Fig. 3. Optimized CBB activation strength enhances biomass and PHA production. **(A)** Predicted effect of varying CBB-mediated CO_2 fixation levels on biomass generation rates from palmitate, as determined by flux balance analysis (FBA) under unlimited O_2 flux. **(B)** Combined effects of CO_2 fixation levels and O_2 flux on biomass generation rates from palmitate, represented as a heatmap. Optimal CO_2 fixation levels (100 % CBB strength) for maximizing biomass generation under specific O_2 flux conditions are highlighted with dashed lines. **(C)** Effect of varying CBB strengths on biomass generation rates from palmitate under defined O_2 fluxes, as predicted by FBA. Practical O_2 flux ranges measured in bioreactor fermentations are shown as dashed lines. **(D)** Transcriptional levels (TPM) of the chromosomal CBB cluster in *C. necator* strains engineered with different CBB activation strengths sampled at 10 h in 2-L fed-batch fermentation. **(E)** Biomass (DCW) accumulation over time in 2-L fed-batch fermentation of engineered *C. necator* strains with different CBB activation strengths. **(F)** PHA production in the same samples as in (E). Data are shown as mean ± SEM, n = 4 per group.

or because excessive CBB flux diverted reducing power and energy away from biomass generation.

We reasoned that real-world constraints could interplay with CBB-mediated CO_2 fixation to affect the optimal CBB strength and its effect on bioproduction. We next examined the impact of CBB activation under defined O_2 supply levels, as oxygen is required as an electron acceptor for reducing equivalents and industrial conditions for aerobic fermentation are usually oxygen-constrained (Garcia-Ochoa and Gomez, 2009; Meadows et al., 2016). Stoichiometric calculations showed a 55 % theoretical increase of PHA productivity under 100 mmol/(L·h) oxygen limit (Table 2). Using an O_2-constrained FBA model to examine the combined effects of O_2 supply and CBB strength on biomass generation, we identified specific levels of CBB-mediated CO_2 fixation (100 % CBB strength) that maximized biomass generation rates at given O_2 fluxes (Fig. 3B). At lower CBB strengths, reducing power remained in surplus and underutilized, while higher-than-optimal CBB strengths resulted in competition for energy, reducing biomass productivity. As O_2 supply increased, more palmitate could be consumed, generating greater amounts of excess reducing power that could be effectively recycled through CBB-mediated CO_2 fixation. This led to both faster biomass generation and higher molar carbon yields overall (Fig. 3B, Fig. S7). Real-world O_2 flux measurements in bioreactor fermentations ranged between 7.42 and 11.53 mmol/gDCW/h, and within this range, enforcing optimal CBB strengths could achieve up to a 13.67 % increase in biomass generation rates at metabolic homeostasis (Fig. 3C). Together, these analyses support CBB-mediated CO_2 fixation as a fine-tunable strategy to recycle excess reducing power at an optimal strength for industrial bioproduction.

To create a genome-integrated strain with optimal CBB activation strength, we designed a library of artificial promoters covering a 100-

fold range of expression levels based on our previously established transcriptional reporter system (Xiang and Li, 2022). By replacing the chromosomal *cbbR*-P*cbbLS* regulatory sequence with these promoters, we created a series of *C. necator* strains spanning a 3450-fold range of *cbb* transcriptional levels (0.77–2653 TPM) during palm oil metabolism, which corresponded to 0.05–194-fold activation relative to wildtype *C. necator* H16G and covered the range of *cbbR**-mediated activation (Figs. 3D and 2A). Bench-scale 2-L fed-batch fermentation of these strains using palm oil revealed that biomass and PHA production were maximized at intermediate CBB activation strengths, exemplified by the cbb4 strain. Specifically, at 32 h, the range of biomass increases observed across the strains was between −18 % and 21 %, while the range of PHA yield increases was between −36 % and 25 %. Strains with either lower or higher CBB activation strengths displayed reduced biomass and PHA yields, confirming that both insufficient and excessive CBB activation can negatively affect productivity (Fig. 3E and F).

3.4. CBB activation improves metabolic efficiency through reducing power recycling and carbon redistribution

Having identified the optimal CBB activation strength, we next investigated its impact on carbon and reducing power metabolism during fed-batch fermentation. RNAseq profiling of cbb4 revealed significant transcriptional upregulation of the *cbb* genes compared to the wildtype H16G, with minimal perturbation to other genes involved in central carbon metabolism (Fig. S2). To further examine metabolic changes, metabolite profiling was conducted at two time points: 10 h (rapid cell division phase) and 32 h (PHA accumulation phase) in a 2-L bioreactor (Fig. S8). While overall metabolite levels showed no significant changes, multiple metabolites associated with the CBB pathway were upregulated, confirming successful activation of the CBB pathway (Fig. 4A, S9). In the wild-type *C. necator* H16G strain, the NADH/NAD ratio significantly increased and the NADPH/NADP ratio decreased from 10 to 32 h, reflecting a reduced energy demand as cells transitioned from division to PHA synthesis (Fig. 4B). Compared to H16G, cbb4 showed a slight but not significant downward trend in these ratios at 10 h. By 32 h, however, both NADH/NAD and NADPH/NADP ratios were significantly lower in cbb4 than in H16G (Fig. 4B), suggesting that CBB activation effectively alleviated reducing power surplus, particularly during PHA synthesis. Additionally, the significant downregulation of stearoyl-CoA and palmitoyl-CoA at both time points indicated enhanced fatty acid oxidation, which can be attributed to the alleviation of reducing power surplus (Fig. 4A–S9). The reduced surplus of NADH and NADPH relieved the inhibition of β-oxidation, thereby accelerating fatty acid breakdown and enabling efficient carbon and energy flow. The reduced levels of 3-hydroxybutyrate (3-HB), likely a degradation product of 3-HB-CoA, suggest that 3-HB-CoA was efficiently redirected toward PHA biosynthesis (Fig. 4A–S9). These results collectively linked the enhanced palm oil consumption and PHA production in cbb4 to improved reducing power recycling mediated by CBB activation.

Since accurate metabolic efficiency measurements are challenging at the 2-L scale due to technical issues including small-scale variations and sampling errors, we next evaluated the metabolic efficiency of cbb4 in the 200-L fed-batch fermentation equipped with exhaust gas composition analysis. At 48 h, cbb4 exhibited a 31 % increase in biomass, a 37 % increase in PHA yield, and a 36 % increase in palm oil consumption, along with an 11 % improvement in the substrate conversion rate compared to H16G (Fig. 4C and D). Notably, cbb4 showed a 12 % reduction in the respiratory quotient (CO_2 emission per O_2 consumption) compared to H16G (Fig. 4E), indicating improved metabolic efficiency. As PHA biosynthesis does not emit CO_2, CO_2 emissions solely reflect cellular metabolic activity. When normalized to residual cell weight (dry cell weight minus PHA), no significant difference in CO_2 emissions was observed between cbb4 and H16G (Fig. S10), suggesting no significant changes in overall cellular decarboxylation activities. However, oxygen consumption per unit of palm oil consumption in cbb4 was 11 % lower than in H16G (Fig. 4F), indicating that a portion of the reducing power generated from palm oil was directed toward CO_2 fixation and PHA synthesis instead of being oxidized through the electron transport chain. Similarly, CO_2 emissions per unit of palm oil consumption were 22 % lower in cbb4 (Fig. 4F), consistent with the notion that less carbon from palm oil was oxidized to CO_2, with a portion being fixed by the activated CBB cycle.

To quantify the carbon flow from palm oil, we conducted a detailed carbon flow analysis. Palm oil-derived carbon was partitioned into cellular components (cellular carbon), PHA production (PHA carbon), CO_2 emissions (CO_2 carbon), and other sinks, including excreted metabolites, etc. (Fig. 4G). This analysis revealed a 6.1 % increase in carbon flow toward PHA biosynthesis, a 3.6 % reduction in carbon allocated to cellular components, and a 3.0 % decrease in carbon lost as CO_2, with no significant changes in other sinks or calculation errors (Fig. 4H).

Together, these findings demonstrated that the activation of the CBB pathway not only alleviated reducing power surplus but also redirected metabolic fluxes toward more efficient carbon utilization, enhancing both metabolic efficiency and PHA production.

3.5. Scalability and performance of cbb4 at industrial scale

The observed improvements in metabolic efficiency and PHA production at the 200-L scale encouraged us to evaluate whether these findings could be translated to larger-scale industrial applications. To this end, we scaled up the fed-batch fermentation to a 15-m^3 bioreactor to assess the performance and scalability of the engineered cbb4 strain under industrially relevant conditions (Fig. 5A). Consistent with the trends observed at the 200-L scale, cbb4 demonstrated significantly higher biomass, PHA yield, and oil consumption compared to the wildtype H16G strain. After 60 h of fermentation, cbb4 achieved a 15 % increase in biomass, a 20 % increase in PHA yield, and an 18 % increase in oil consumption relative to H16G (Fig. 5B). The productivity of cbb4 remained consistently higher than that of H16G across all tested scales (2-L, 200-L, and 15-m^3), with the highest productivity observed at the 200-L scale (Fig. 5C). The slight decline in productivity at the 15-m^3 scale was likely due to mass transfer limitations inherent in larger fermenters. Similar to the 200-L scale, the 15-m^3 fed-batch fermentation of cbb4 exhibited a higher substrate conversion rate, lower respiratory quotient, and reduced O_2 consumption and CO_2 emission per unit of palm oil consumed, indicating enhanced metabolic efficiency at the industrial scale (Fig. S11).

Overall, these results demonstrated the robustness and scalability of the CBB activation strategy, confirming its value for enhancing industrial bioproduction.

4. Discussion

Balancing of reducing power is a critical challenge in the bioproduction of valuable compounds from highly reduced carbon sources like palm oil. Palm oil metabolism generates an excess of reducing power, leading to redox imbalances and metabolic inefficiencies. By repurposing the endogenous Calvin-Benson-Bassham (CBB) cycle in *C. necator* to recycle reducing power for CO_2 fixation, we demonstrated a simple and effective strategy to mitigate this challenge. This study makes several significant contributions by not only achieving the first quantitative identification of excess reducing power in palm oil metabolism but also demonstrating how energy recycling achieved through optimized level of CBB cycle activation can effectively enhance biomass accumulation and PHA production. A key advantage of our approach is the integration of computational metabolic modeling to guide strain engineering. By utilizing flux balance analysis (FBA), we were able to rationally predict and optimize pathway modifications that enhance palm oil utilization efficiency and PHA biosynthesis. This model-driven approach is broadly applicable across various metabolic engineering efforts, as similar predictive frameworks have been employed to

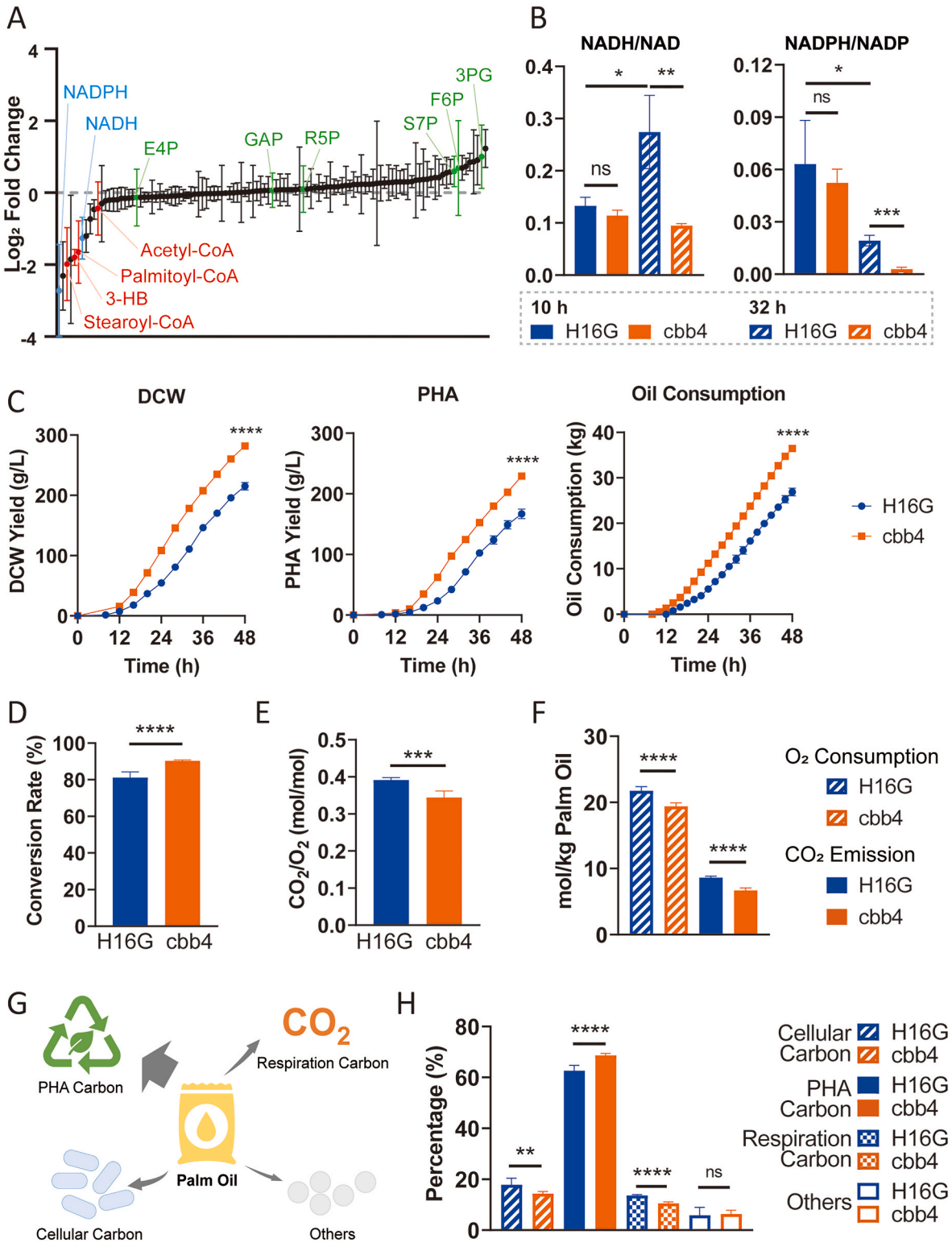

Fig. 4. CBB activation enhances biomass and PHA production while alleviating reducing power surplus. **(A)** Log_2 fold changes in metabolite levels of cbb4 relative to H16G at 32 h in a 2-L bioreactor. Metabolites associated with the CBB pathway are shown in green, PHA synthesis metabolites in red, and reducing power metabolites in blue. **(B)** NADH/NAD and NADPH/NADP ratios of H16G and cbb4 at 10 h (rapid growth phase) and 32 h (PHA accumulation phase) in a 2-L bioreactor. **(C)** Biomass (DCW), PHA yield, and oil consumption curves of H16G and cbb4 in the 200-L fed-batch fermentation. **(D)** Comparison of mass conversion rate (oil to PHA) between H16G and cbb4 in the 200-L fed-batch fermentation. **(E)** Comparison of respiration quotient between H16G and cbb4 in 200-L fed-batch fermentation. **(F)** Comparison of O_2 consumption and CO_2 emission between H16G and cbb4 in the 200-L fed-batch fermentation, normalized to palm oil consumption. **(G)** Illustration of carbon flow from palm oil to respiration, cellular component, and PHA production. **(H)** Comparison of carbon flow between H16G and cbb4 in the 200-L fed-batch fermentation. Data are shown as mean ± SEM, n = 3 for (A)–(B), n = 6 for (C)–(H). Statistical significance was determined using a two-tailed Student's t-test (ns not significant, *$p < 0.05$, **$p < 0.01$, ***$p < 0.001$, ****$p < 0.0001$). (For interpretation of the references to colour in this figure legend, the reader is referred to the Web version of this article.)

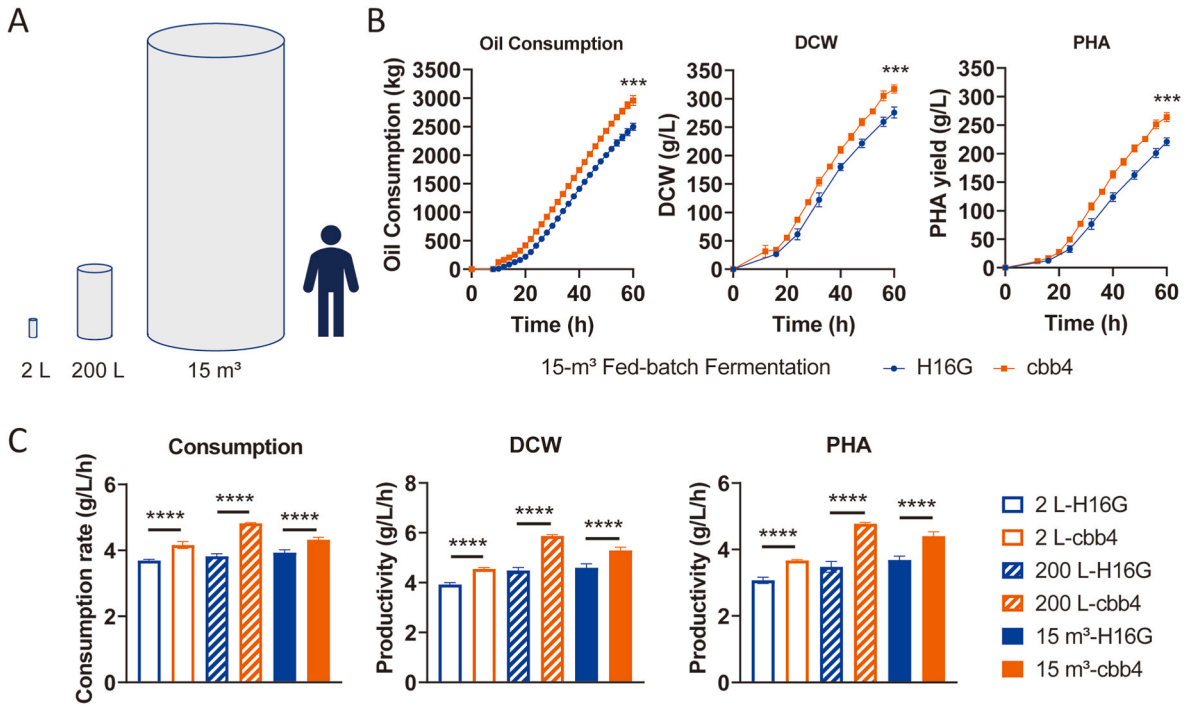

Fig. 5. Scalability of cbb4 modification in the 15-m^3 fed-batch fermentation. **(A)** Illustration of 2-L, 200-L and 15-m^3 bioreactors. **(B)** Oil consumption, biomass (DCW) and PHA yield curves of H16G and cbb4 strains cultured in the 15-m^3 fed-batch fermentation. **(C)** Comparison of oil consumption, DCW and PHA yield between H16G and cbb4 in the 2-L, 200-L and 15-m^3 fed-batch fermentations. Data are shown as mean ± SEM, n ≥ 4 per group. Statistical significance was determined using a two-tailed Student's t-test (****$p < 0.0001$).

optimize carbon flux and redox balance in diverse microbial systems (Raman and Chandra, 2009; Nogales et al., 2013; Kuriya and Araki, 2020; Vikromvarasiri et al., 2023). The successful implementation of FBA-guided strain design in this study demonstrates its potential as a powerful tool for improving industrial bioproduction. Beyond PHA biosynthesis, such computational approaches could be extended to other metabolic pathways, enabling efficient production of a wide range of biochemicals through targeted metabolic rewiring. To validate these computational predictions in real-world conditions, we experimentally engineered *C. necator* strains and scaled up fermentation processes. By upscaling to 15-m^3 production level, we validate the robustness and scalability of this metabolic engineering strategy.

The plasmid-based *cbbR* system* has inherent limitations, necessitating a more robust approach for CBB activation. A genome-integrated biorthogonal-designed strain presents several advantages over plasmid-based activation. First, single-copy genomic integration allows for precise tuning of CBB activation strength, preventing plasmid copy number variations that could lead to inconsistent or excessive activation. Second, biorthogonal activation of CBB transcription bypasses endogenous *cbbR*-related regulatory constraints, increasing the stability and robustness of the engineered CBB pathway. Finally, genome integration enhances strain stability, eliminating concerns of plasmid loss, particularly under industrial-scale conditions. By employing this genomically integrated biorthogonal strategy, optimal tuning of CBB activation strength was crucial for maximizing productivity, as both insufficient and excessive activation impaired metabolic efficiency. Insufficient activation limited reducing power recycling, causing NADPH accumulation and metabolic inefficiencies, such as inhibited β-oxidation, while excessive activation diverted essential resources such as NADPH and ATP away from biosynthetic processes. At optimal activation strength, biomass and PHA yields increased by 15 % and 20 %, respectively, at the industrial scale, underscoring the importance of precise regulation of CBB fluxes to maintain metabolic balance. The dynamic regulation of redox balance further highlights the adaptability of this strategy. While flux balance analysis (FBA) predictions suggested that CBB activation could efficiently recycle reducing power during biomass accumulation, our results indicate that its effects were more pronounced during PHA biosynthesis. During the rapid biomass accumulation phase (10 h), high energy demands for cell growth efficiently consumed NADH, minimizing the impact of CBB activation on NAD(P)H ratios. By 32 h when active PHA synthesis consumed NADPH, leaving NADH in excess, the activated CBB cycle effectively recycled the excess reducing power through CO_2 fixation, aligning metabolic fluxes with cellular priorities and optimizing redox balance and productivity. Together with the reduced oxygen consumption and carbon emission reflecting an improved metabolic efficiency at industrial scale, these findings demonstrate the scalability and robustness of CBB activation and highlight its potential to integrate CO_2 fixation pathways into industrial bioprocesses, enabling reduced carbon footprints while enhancing bioproduction efficiency.

While CO_2 fixation plays a crucial role in our engineered metabolic pathway, it is important to consider the feasibility of supplying external CO_2 in large-scale fermentation. Although additional CO_2 could potentially enhance PHA production, the economic and logistical challenges make this approach impractical for industrial applications. Furthermore, previous studies have reported inhibitory effects of high CO_2 concentrations on *C. necator*. Shang et al. (2003) concluded that excessive CO_2 negatively impacts both growth and PHA synthesis. This suggests that supplying additional CO_2 may not always enhance productivity and could even hinder microbial performance under certain conditions. Additionally, although *C. necator* is a facultative autotroph capable of using CO_2 as the sole carbon source, autotrophic PHA production suffers from inherently low growth rates and productivity (Li et al., 2020; Tanaka et al., 2021; Kim et al., 2022), making it unsuitable for commercial-scale biosynthesis. Instead, our strategy leverages CO_2 fixation to optimize heterotrophic production, enabling the metabolic benefits of CBB activation while preserving the high efficiency of plant oil-driven PHA fermentation.

The CBB cycle, although not the most carbon-efficient CO_2 fixation pathway, offers distinct advantages for industrial bioproduction. Specifically, the CBB pathway is oxygen-insensitive, enabling it to operate

under the aerobic conditions typical of large-scale fermentation processes. In contrast, many alternative CO_2 fixation pathways, such as the Wood-Ljungdahl pathway and the Reductive Glycine pathway, are strictly anaerobic, making them less suitable for these environments. Moreover, the CBB cycle is endogenous to *C. necator*, which simplifies its activation and integration without the need to introduce foreign genetic elements. However, activating the entire native *cbb* cluster as a whole may lead to limited control over individual pathway components, potentially resulting in suboptimal flux distributions or imbalances in resource allocation, limiting the overall efficiency of CO_2 fixation and downstream biosynthesis. By combining mechanistic knowledge of the native CBB pathway with advanced synthetic biology tools, *cbb* cluster refactoring represents a promising future direction to maximize CO_2 fixation efficiency, reduce resource wastage, and further improve the productivity and robustness of industrial microbial systems (Temme et al., 2012). Additionally, while the CBB cycle was the optimal choice for this study, a systematic comparison of various CO_2 fixation pathways—including efforts to overcome oxygen sensitivity—remains an important direction for future research to identify the most suitable strategies for specific bioproduction contexts.

Beyond PHA production, the approach described here has broader implications for sustainable bioproduction. The integration of CO_2 fixation pathways to recycle reducing power offers a versatile solution for enhancing the synthesis of other value-added compounds, such as 3-hydroxypropionic acid (Salinas et al., 2022) and biofuels (Panich et al., 2021).

5. Conclusion

In summary, our study demonstrates a novel strategy to address the challenges of excess reducing power using palm oil as carbon source by activating the CBB cycle in *C. necator*. By redirecting surplus reducing power to CO_2 fixation, the strategy effectively alleviates redox imbalance, reduces oxygen consumption, and enhances PHA production. Precise tuning of CBB activation strength was critical, with optimal activation maximizing productivity while avoiding inefficiencies from under- or over-activation. The scalability and robustness of this approach were validated in both 200-L and 15-m^3 bioreactors, highlighting its industrial applicability. These findings provide a framework for integrating metabolic engineering and CO_2 fixation to advance sustainable bioproduction, reduce carbon footprints, and enhance industrial efficiency.

CRediT authorship contribution statement

Jing Feng: Validation, Methodology, Investigation. **Xueshan Li:** Investigation, Data curation. **Xin Teng:** Writing – original draft, Visualization, Data curation. **Dingding Fan:** Software, Formal analysis. **Jin Yin:** Investigation. **Yanci Qiu:** Investigation. **Ziling Yi:** Investigation. **Li Chen:** Supervision. **Haoqian M. Zhang:** Supervision, Conceptualization. **Chitong Rao:** Writing – review & editing, Writing – original draft, Supervision, Conceptualization.

Data availability statement

The RNA-seq raw data generated in this study are not publicly available due to proprietary restrictions and commercial sensitivity. However, to ensure transparency, the analyzed RNA sequencing expression profiles, metabolic models and analysis scripts are provided in detail in the GitHub repository at https://github.com/DingDingFan/CBB_paper/.

Funding

This work was funded by Bluepha Co., Ltd., and STCSM grants 24QB2703700 and 2023PJD06.

Conflict of interest

Jing Feng, Xin Teng, Dingding Fan, Jin Yin, Yanci Qiu, Ziling Yi, Haoqian M. Zhang, and Chitong Rao are employees at Bluepha Co., Ltd.

Acknowledgement

We thank Ms Cheng R. at the metabolomics facility of the Shanghai Key Laboratory of Metabolic Remodeling and Health, Fudan University for the technical support.

Appendix A. Supplementary data

Supplementary data to this article can be found online at https://doi.org/10.1016/j.ymben.2025.04.009.

Data availability

The RNA-seq raw data are not publicly available due to commercial sensitivity. However, the analyzed RNA sequencing expression profiles are provided at https://github.com/DingDingFan/CBB_paper/

References

Bowien, B., Kusian, B., 2002. Genetics and control of CO(2) assimilation in the chemoautotroph Ralstonia eutropha. Arch. Microbiol. 178, 85–93.
Budde, C.F., Riedel, S.L., Hübner, F., Risch, S., Popović, M.K., Rha, C., Sinskey, A.J., 2011. Growth and polyhydroxybutyrate production by Ralstonia eutropha in emulsified plant oil medium. Appl. Microbiol. Biotechnol. 89, 1611–1619.
Bulović, A., Fischer, S., Dinh, M., Golib, F., Liebermeister, W., Poirier, C., Tournier, L., Klipp, E., Fromion, V., Goelzer, A., 2019. Automated generation of bacterial resource allocation models. Metab. Eng. 55, 12–22.
Ciebiada, M., Kubiak, K., Daroch, M., 2020. Modifying the cyanobacterial metabolism as a key to efficient biopolymer production in photosynthetic microorganisms. Int. J. Mol. Sci. 21, 7204.
Dangel, A.W., Tabita, F.R., 2015. Amino acid substitutions in the transcriptional regulator CbbR lead to constitutively active CbbR proteins that elevate expression of the cbb CO2 fixation operons in Ralstonia eutropha (Cupriavidus necator) and identify regions of CbbR necessary for gene activation. Microbiology (Read.) 161, 1816–1829.
Dobin, A., Davis, C.A., Schlesinger, F., Drenkow, J., Zaleski, C., Jha, S., Batut, P., Chaisson, M., Gingeras, T.R., 2013. STAR: ultrafast universal RNA-seq aligner. Bioinformatics 29, 15–21.
Dugar, D., Stephanopoulos, G., 2011. Relative potential of biosynthetic pathways for biofuels and bio-based products. Nat. Biotechnol. 29, 1074–1078.
Ebrahim, A., Lerman, J.A., Palsson, B.O., Hyduke, D.R., 2013. COBRApy: COnstraints-based reconstruction and analysis for Python. BMC Syst. Biol. 7, 74.
Ewels, P.A., Peltzer, A., Fillinger, S., Patel, H., Alneberg, J., Wilm, A., Garcia, M.U., Di Tommaso, P., Nahnsen, S., 2020. The nf-core framework for community-curated bioinformatics pipelines. Nat. Biotechnol. 38, 276–278.
Garcia-Ochoa, F., Gomez, E., 2009. Bioreactor scale-up and oxygen transfer rate in microbial processes: an overview. Biotechnol. Adv. 27, 153–176.
Gibson, D.G., Young, L., Chuang, R.-Y., Venter, J.C., Hutchison, C.A., Smith, H.O., 2009. Enzymatic assembly of DNA molecules up to several hundred kilobases. Nat. Methods 6, 343–345.
Gruber, S., Schwab, H., Heidinger, P., 2017. CbbR and RegA regulate cbb operon transcription in Ralstonia eutropha H16. J. Biotechnol. 257, 78–86.
Grzeszik, C., Jeffke, T., Schäferjohann, J., Kusian, B., Bowien, B., 2000. Phosphoenolpyruvate is a signal metabolite in transcriptional control of the cbb CO2 fixation operons in Ralstonia eutropha. J. Mol. Microbiol. Biotechnol. 2, 311–320.
Insomphun, C., Mifune, J., Orita, I., Numata, K., Nakamura, S., Fukui, T., 2014. Modification of β-oxidation pathway in Ralstonia eutropha for production of poly(3-hydroxybutyrate-co-3-hydroxyhexanoate) from soybean oil. J. Biosci. Bioeng. 117, 184–190.
Jahn, M., Crang, N., Janasch, M., Hober, A., Forsström, B., Kimler, K., Mattausch, A., Chen, Q., Asplund-Samuelsson, J., Hudson, E.P., 2021. Protein allocation and utilization in the versatile chemolithoautotroph Cupriavidus necator. Elife 10, e69019.
Jiang, G., Hill, D.J., Kowalczuk, M., Johnston, B., Adamus, G., Irorere, V., Radecka, I., 2016. Carbon sources for polyhydroxyalkanoates and an integrated biorefinery. Int. J. Mol. Sci. 17, 1157.
Kim, S., Jang, Y.J., Gong, G., Lee, S.-M., Um, Y., Kim, K.H., Ko, J.K., 2022. Engineering Cupriavidus necator H16 for enhanced lithoautotrophic poly(3-hydroxybutyrate) production from CO2. Microb. Cell Fact. 21, 231.
Koller, M., Braunegg, G., 2018. Advanced approaches to produce polyhydroxyalkanoate (PHA) biopolyesters in a sustainable and economic fashion. The EuroBiotech Journal 2, 89–103.

Kuriya, Y., Araki, M., 2020. Dynamic flux balance analysis to evaluate the strain production performance on shikimic acid production in Escherichia coli. Metabolites 10, 198.
Kusian, B., Bednarski, R., Husemann, M., Bowien, B., 1995. Characterization of the duplicate ribulose-1,5-bisphosphate carboxylase genes and cbb promoters of Alcaligenes eutrophus. J. Bacteriol. 177, 4442–4450.
Li, Z., Xin, X., Xiong, B., Zhao, D., Zhang, X., Bi, C., 2020. Engineering the Calvin–Benson–Bassham cycle and hydrogen utilization pathway of Ralstonia eutropha for improved autotrophic growth and polyhydroxybutyrate production. Microb. Cell Fact. 19, 228.
Martinez-Val, A., Bekker-Jensen, D.B., Hogrebe, A., Olsen, J.V., 2021. Data processing and analysis for DIA-based PhosphoproteomicsPhosphoproteomics using SpectronautSpectronaut. In: Cecconi, D. (Ed.), Proteomics Data Analysis. Springer US, New York, NY, pp. 95–107.
Meadows, A.L., Hawkins, K.M., Tsegaye, Y., Antipov, E., Kim, Y., Raetz, L., Dahl, R.H., Tai, A., Mahatdejkul-Meadows, T., Xu, L., Zhao, L., Dasika, M.S., Murarka, A., Lenihan, J., Eng, D., Leng, J.S., Liu, C.-L., Wenger, J.W., Jiang, H., Chao, L., Westfall, P., Lai, J., Ganesan, S., Jackson, P., Mans, R., Platt, D., Reeves, C.D., Saija, P.R., Wichmann, G., Holmes, V.F., Benjamin, K., Hill, P.W., Gardner, T.S., Tsong, A.E., 2016. Rewriting yeast central carbon metabolism for industrial isoprenoid production. Nature 537, 694–697.
Nogales, J., Gudmundsson, S., Thiele, I., 2013. Toward systems metabolic engineering in cyanobacteria. Bioengineered 4, 158–163.
Orita, I., Iwazawa, R., Nakamura, S., Fukui, T., 2012. Identification of mutation points in *Cupriavidus necator* NCIMB 11599 and genetic reconstitution of glucose-utilization ability in wild strain H16 for polyhydroxyalkanoate production. J. Biosci. Bioeng. 113, 63–69.
Palmieri, S., Tittarelli, F., Sabbatini, S., Cespi, M., Bonacucina, G., Eusebi, A.L., Fatone, F., Stipa, P., 2021. Effects of different pre-treatments on the properties of polyhydroxyalkanoates extracted from sidestreams of a municipal wastewater treatment plant. Sci. Total Environ. 801, 149633.
Panich, J., Fong, B., Singer, S.W., 2021. Metabolic engineering of *Cupriavidus necator* H16 for sustainable biofuels from CO2. Trends Biotechnol. 39, 412–424. Special Issue: Bioconversion of C1 Products and Feedstocks.
Park, H., He, H., Yan, X., Liu, X., Scrutton, N.S., Chen, G.-Q., 2024. PHA is not just a bioplastic. Biotechnol. Adv. 71, 108320.
Patro, R., Duggal, G., Love, M.I., Irizarry, R.A., Kingsford, C., 2017. Salmon provides fast and bias-aware quantification of transcript expression. Nat. Methods 14, 417–419.
Pearcy, N., Garavaglia, M., Millat, T., Gilbert, J.P., Song, Y., Hartman, H., Woods, C., Tomi-Andrino, C., Bommareddy, R.R., Cho, B.-K., Fell, D.A., Poolman, M., King, J.R., Winzer, K., Twycross, J., Minton, N.P., 2022. A genome-scale metabolic model of Cupriavidus necator H16 integrated with TraDIS and transcriptomic data reveals metabolic insights for biotechnological applications. PLoS Comput. Biol. 18, e1010106.
Rai, P., Mehrotra, S., Priya, S., Gnansounou, E., Sharma, S.K., 2021. Recent advances in the sustainable design and applications of biodegradable polymers. Bioresour. Technol. 325, 124739.
Raman, K., Chandra, N., 2009. Flux balance analysis of biological systems: applications and challenges. Brief. Bioinform. 10, 435–449.
Salinas, A., McGregor, C., Irorere, V., Arenas-López, C., Bommareddy, R.R., Winzer, K., Minton, N.P., Kovács, K., 2022. Metabolic engineering of Cupriavidus necator H16 for heterotrophic and autotrophic production of 3-hydroxypropionic acid. Metab. Eng. 74, 178–190.
Schreier, T.B., Hibberd, J.M., 2019. Variations in the Calvin–Benson cycle: selection pressures and optimization? J. Exp. Bot. 70, 1697–1701.
Shang, L., Jiang, M., Ryu, C.H., Chang, H.N., Cho, S.H., Lee, J.W., 2003. Inhibitory effect of carbon dioxide on the fed-batch culture of Ralstonia eutropha: evaluation by CO2 pulse injection and autogenous CO2 methods. Biotechnol. Bioeng. 83, 312–320.
Sheu, D.-S., Lee, C.-Y., 2004. Altering the substrate specificity of polyhydroxyalkanoate synthase 1 derived from Pseudomonas putida GPo1 by localized semirandom mutagenesis. J. Bacteriol. 186, 4177–4184.
Shimizu, R., Chou, K., Orita, I., Suzuki, Y., Nakamura, S., Fukui, T., 2013. Detection of phase-dependent transcriptomic changes and Rubisco-mediated CO2 fixation into poly (3-hydroxybutyrate) under heterotrophic condition in Ralstonia eutropha H16 based on RNA-seq and gene deletion analyses. BMC Microbiol. 13, 169.
Shimizu, R., Dempo, Y., Nakayama, Y., Nakamura, S., Bamba, T., Fukusaki, E., Fukui, T., 2015. New insight into the role of the Calvin cycle: reutilization of CO2 emitted through sugar degradation. Sci. Rep. 5, 11617.
Simon, R., Priefer, U., Pühler, A., 1983. A broad host range mobilization system for in vivo genetic engineering: transposon mutagenesis in gram negative bacteria. Nat. Biotechnol. 1, 784–791.
Sudesh, K., Bhubalan, K., Chuah, J.-A., Kek, Y.-K., Kamilah, H., Sridewi, N., Lee, Y.-F., 2011. Synthesis of polyhydroxyalkanoate from palm oil and some new applications. Appl. Microbiol. Biotechnol. 89, 1373–1386.
Tanaka, K., Yoshida, K., Orita, I., Fukui, T., 2021. Biosynthesis of poly(3-hydroxybutyrate-co-3-hydroxyhexanoate) from CO2 by a recombinant cupriavidusnecator. Bioengineering 8, 179.
Tang, R., Weng, C., Peng, X., Han, Y., 2020. Metabolic engineering of Cupriavidus necator H16 for improved chemoautotrophic growth and PHB production under oxygen-limiting conditions. Metab. Eng. 61, 11–23.
Temme, K., Zhao, D., Voigt, C.A., 2012. Refactoring the nitrogen fixation gene cluster from Klebsiella oxytoca. Proc. Natl. Acad. Sci. 109, 7085–7090.
Vikromvarasiri, N., Noda, S., Shirai, T., Kondo, A., 2023. Investigation of two metabolic engineering approaches for (R,R)-2,3-butanediol production from glycerol in Bacillus subtilis. J. Biol. Eng. 17, 3.
Wang, Y., Yin, J., Chen, G.-Q., 2014. Polyhydroxyalkanoates, challenges and opportunities. Curr. Opin. Biotechnol. 30, 59–65. Chemical biotechnology • Pharmaceutical biotechnology.
Windhövel, U., Bowien, B., 1991. Identification of cfxR, an activator gene of autotrophic CO2 fixation in Alcaligenes eutrophus. Mol. Microbiol. 5, 2695–2705.
Xiang, R., Li, T., 2022. Promoter Library and Method for Constructing Expression Systems with Different Intensities in Bacteria.
Yañez, L., Conejeros, R., Vergara-Fernández, A., Scott, F., 2020. Beyond intracellular accumulation of polyhydroxyalkanoates: chiral hydroxyalkanoic acids and polymer secretion. Front. Bioeng. Biotechnol. 8.
Zhang, Z., TeSlaa, T., Xu, X., Zeng, X., Yang, L., Xing, G., Tesz, G.J., Clasquin, M.F., Rabinowitz, J.D., 2021. Serine catabolism generates liver NADPH and supports hepatic lipogenesis. Nat. Metab. 3, 1608–1620.